Field-induced quasi-particle tunneling in the nodal-line semimetal HfSiS revealed by de Haas-van Alphen quantum oscillations

C. S. A. Müller,[1,2,*] M. R. van Delft,[1,2] T. Khouri,[1,2] M. Breitkreiz,[3] L. M. Schoop,[4] A. Carrington,[5] N. E. Hussey,[1,2,5] and S. Wiedmann[1,2,†]

[1]*High Field Magnet Laboratory (HFML-EMFL), Radboud University, Toernooiveld 7, Nijmegen 6525 ED, Netherlands*
[2]*Radboud University, Institute for Molecules and Materials, Nijmegen 6525 AJ, Netherlands*
[3]*Dahlem Center for Complex Quantum Systems and Fachbereich Physik, Freie Universität Berlin, 14195 Berlin, Germany*
[4]*Department of Chemistry, Princeton University, Princeton, New Jersey 08544, USA*
[5]*H. H. Wills Physics Laboratory, University of Bristol, Tyndall Avenue, Bristol BS8 1TL, UK*

(Received 18 July 2022; accepted 29 August 2022; published 4 October 2022)

We present a de Haas–van Alphen quantum oscillation study of the Dirac nodal-line semimetal HfSiS up to 32 T to unravel the structure of the high-frequency magnetic breakdown spectrum that was previously obscured in transport experiments. Despite a threefold enhanced gap between adjacent electron and hole pockets relative to the sister compound ZrSiS, a large number of large-area magnetic breakdown orbits enclosing the nodal-loop are identified. All breakdown orbits are assigned by extracting their cyclotron masses. Moreover, one additional low-frequency magnetic breakdown orbit, previously absent in ZrSiS, is observed and attributed to the larger spin-orbit interaction in HfSiS.

DOI: 10.1103/PhysRevResearch.4.043008

I. INTRODUCTION

Over the past few years, nodal-line semimetals (NLSMs) have been one of the most intensely studied, ever-growing topological compounds [1]. In contrast to Weyl and Dirac semimetals where distinct point-like band crossings occur in the Brillouin zone (BZ), NLSMs are materials in which conduction and valence bands touch each other along a closed trajectory, a line or a loop, in momentum space [2]. They also have the potential to become a platform for investigating correlation effects in topological matter [3–5].

Particular attention has been paid to NLSMs with the general formula *M*Si*X* (*M* = Zr, Hf and *X* = S, Se, Te), which have a PbFCl-type structure. Among the Zr family, ZrSiS is considered to be a textbook material with its Fermi surface (FS) composed uniquely of linearly dispersing bands that extend over a large energy range [6]. The underlying band structure, topology, and charge carrier properties were investigated by angle-resolved photoemission, electronic transport, and quantum oscillation (QO) experiments [6–13]. Evidence for sizable electronic correlations in ZrSiS was observed in a number of experimental and theoretical studies [14,15], while superconducivity induced by a nonsuperconducting metallic tip was also reported [16].

The particular arrangement of the FS pockets in this family of materials also allows for the observation of magnetic breakdown (MB), a phenomenon that reveals itself in QO experiments [17]. Above a threshold magnetic field, i.e., the breakdown field, quasi-particle tunneling occurs between adjacent pockets of the FS leading to a plethora of additional QO frequencies corresponding to either a linear combination of closed orbits around adjacent pockets or to large orbits enclosing an entire nodal-loop in the BZ (high-frequency MB in the *ZRA* high-symmetry plane) [14,18]. The observation of MB has only been demonstrated in ZrSiS, while its evidence is still lacking in other members of the ZrSi*X* material family, such as ZrSiSe and ZrSiTe [12].

NLSMs of the *M*Si*X* family with *M* = Hf have also been much less studied until now [19–22]. Yet their investigation is of fundamental importance as the spin-orbit interaction (SOI) in Hf-based systems is stronger, which, apart from changes in the band structure, also leads to a threefold enhanced gap size in momentum space between adjacent pockets in the *ZRA* high-symmetry plane [19]. Despite this enhanced gap, MB was observed in HfSiS, in particular, the "figure-of-eight" breakdown orbit that encloses one electron pocket and one hole pocket in Shubnikov–de Haas (SdH) QO experiments [19]. While some features related to high-frequency MB had already been identified, a quantitative analysis has not yet been performed due to a lack of resolution in previous experiments [19].

In this paper, we report on de Haas–van Alphen (dHvA) QOs in the NLSM HfSiS originating from individual electron and hole pockets, as well as MB orbits that encircle either the entire Dirac nodal-loop or adjacent electron and hole pockets. We assign all high-frequency QOs to MB orbits in the ZRA high-symmetry plane by extracting their cyclotron masses

*claudius.mueller@ru.nl
†steffen.wiedmann@ru.nl

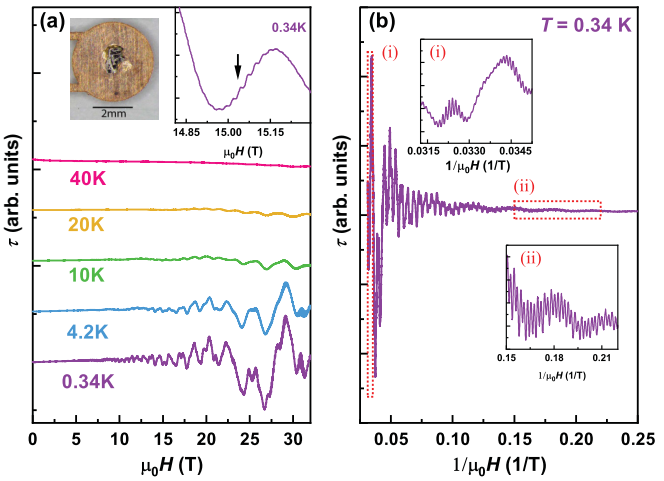

FIG. 1. (a) Torque τ as a function of the magnetic field for chosen temperatures between 0.34 and 40 K up to 32 T with $\mu_0 \mathbf{H} \parallel c$. Curves are offset for clarity. The upper-left inset shows an image of an HfSiS single crystal on a cantilever. The upper-right inset shows the onset of high-frequency QOs for $T = 0.34$ K (indicated with the black arrow). (b) τ as a function of $1/\mu_0 H$ at 0.34 K illustrating the complex QO pattern highlighted by the insets (i) and (ii).

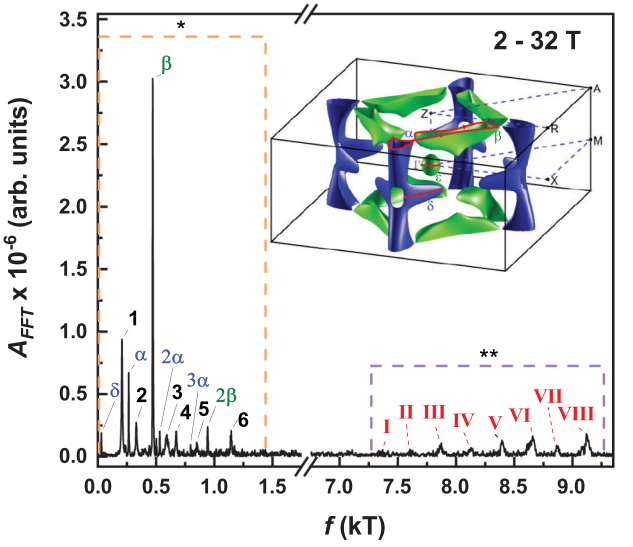

FIG. 2. FFT of the dHvA QOs at $T = 0.34$ K in the range from 2–32 T. Two regimes are observed: for $f < 1.5$ kT, fundamental extremal orbits (Greek letters), their harmonics and low-frequency MB orbits (1–6); for $f > 7$ kT, multiple peaks, labeled with Roman numerals I–VIII that correspond to high-frequency MB orbits in the *ZRA* plane. The inset illustrates the FS calculated with DFT including spin-orbit interaction.

from temperature-dependent measurements. Furthermore, we observe a multitude of low-frequency MB QOs, previously absent in SdH measurements, and determine their respective cyclotron masses enabeling us to make a complete assignment for all MB orbits. The obtained results on MB are compared to the well-studied compound ZrSiS.

II. EXPERIMENTAL DETAILS AND ANALYSIS

The dHvA quantum oscillations of a single crystal sample were measured using capacitive torque magnetometry. Details on the sample synthesis and characterization can be found in the Supplemental Material (SM) [23]. The sample was glued on top of a copper-beryllium plate, see upper-left inset of Fig. 1(a), and the capacitance between two plates was measured with an analog capacitance bridge with a frequency operating at 50 kHz. Torque magnetometry experiments were performed on a rotating stage and cooled in a ^{3}He system with a base temperature of 0.3 K. The field measurements were carried out in a resistive Bitter magnet at the High Field Magnet Laboratory (HFML), Nijmegen, The Netherlands, with a maximum field strength of 35 T. The sample itself was placed a couple of centimeters outside of the field center resulting in a maximum field of 32 T at the sample position so that the parallel and perpendicular magnetization components contributed to the signal. All fast Fourier transforms (FFTs) presented here are analyzed using the Hann window function with an appropriate zero-padding.

III. QUANTUM OSCILLATION SPECTRUM AND FERMI SURFACE

In Fig. 1(a), a series of torque τ sweeps as a function of the magnetic field $\mu_0 H$ on a HfSiS single crystal at different temperatures between 0.34 and 40 K is shown. The magnetic field is applied parallel to the c-axis of the crystal ($\mu_0 H \parallel c$-axis), which will be regarded as a tilt angle $\theta = 0°$. With decreasing temperature, HfSiS displays a complex QO spectrum with high-frequency QOs developing around 15 T [see upper-right inset of Fig. 1(a)] that are ascribed to MB in the *ZRA* plane of the FS of HfSiS, shown in the inset of Fig. 2. The QOs spectrum in the chosen field ranges as a function of the inverse magnetic field at $T = 0.34$ K is shown in Fig. 1(b) and in panels (i) and (ii).

The FFT analysis of the 0.34 K sweep in the range of 2–32 T is shown in Fig. 2. The observed frequencies, f, in the FFT spectra are related to the extremal momentum-space area A_f of the individual pockets via the Onsager relation $f = (\hbar/2\pi e)A_f$ [17]. Three fundamental orbits of the FS are assigned and labeled as $\alpha = 265$ T, $\beta = 470$ T, and $\delta = 30$ T (summarized in Table I) in perfect agreement with the SdH frequencies [19]. Harmonics 2α, 3α, and 2β are also observed. A three-dimensional (3D) representation of the FS of HfSiS, calculated by density functional theory (DFT) (for details see the SM), is displayed in the inset of Fig. 2. Like in ZrSiS [14,18] the FS contains adjacent electron and hole

TABLE I. Identified fundamental orbits, extracted frequencies from Fig. 2, and extracted cyclotron masses from Fig. S1 [23] compared to the frequencies and cyclotron masses from the DFT calculations. Harmonics $(p \cdot \alpha)$, $(n \cdot \beta)$ are omitted.

Orbit	f (T)	m_c (m_e)	f_{DFT} (T)	$m_{c;\mathrm{DFT}}$ (m_e)
δ	30	0.17 ± 0.01	38	
α	265	0.18 ± 0.01	294	0.17
β	470	0.52 ± 0.01	631	0.63

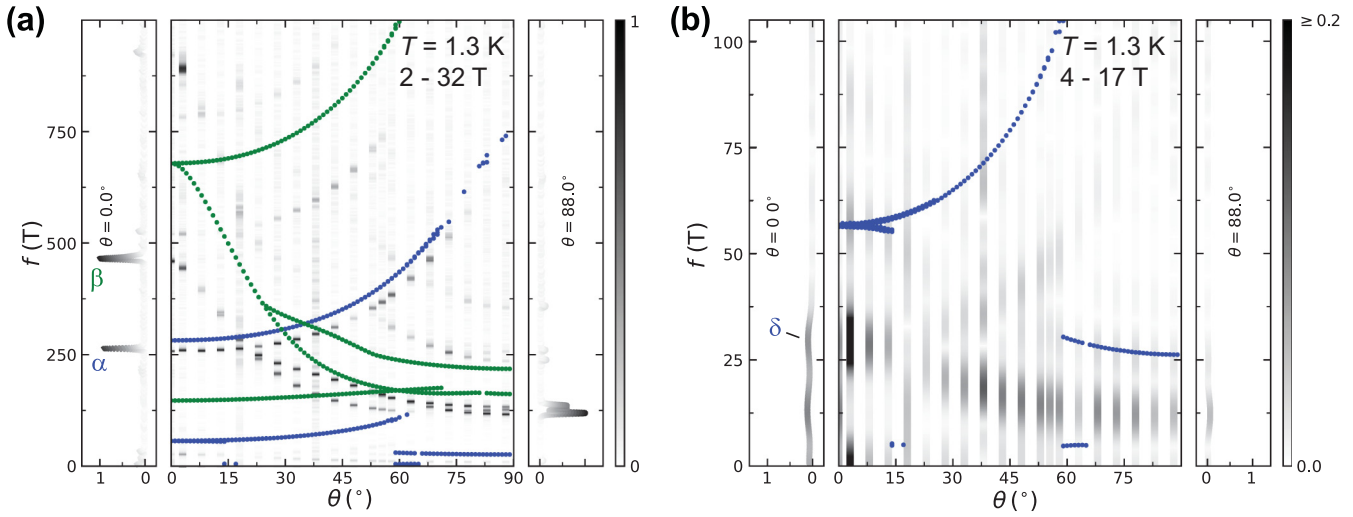

FIG. 3. Fast Fourier transforms of the angle dependence of the measured HfSiS sample for two different field ranges (a) 2–32 T and (b) 4–17 T at $T = 1.3$ K. The left and right panels in (a) and (b) show the FFTs of the two angles $\theta = 0^\circ$ and $\theta = 88^\circ$, respectively, and fundamental orbits are labeled by their respective greek letter as done in Fig. 2 of the main text. The middle panels show a quasi-3D map of all FFT spectra acquired for each angle, where the FFT amplitude determines the opaqueness. Also shown in the middle panels is the angle dependence acquired from DFT calculations, with blue indicating the dispersion of the hole-like parts of the Fermi surface and green the one for the electron-like parts. The colorbar on the right then indicates the mapping of FFT amplitudes to opaqueness. For clarity, each curve at a specific angle is normalized to its maximum value and in (b) points with amplitudes above 0.2 are mapped to full opaqueness.

pockets in the *ZRA* high-symmetry plane, located at the top of the BZ, with a gap between them due to SOI. The minimum gap size here is $\Delta k = 13 \times 10^{-3}$ 1/Å [19], 2.7 times larger than the one of ZrSiS [14,18].

To determine which experimentally observed individual orbits belong to the hole-/electron-like pockets of the FS, we measured the dependence of the QO frequencies on the tilt angle θ, where the sample was rotated from $\mu_0 H \parallel c$ to $\mu_0 H \parallel ab$ and the experimental angle dependence was compared to the one obtained from DFT calculations, consistent with Ref. [19]. The angle dependence of the dHvA QOs of HfSiS is shown in Fig. 3. Figure 3(a) shows the angle dependence in the field range of 2–32 T, the same range as used in Fig. 2, but at a temperature of $T = 1.3$ K. The tilt angle θ is defined as the angle between the c-axis and the direction of the applied magnetic field $\mu_0 H$. In contrast to the FFT of the $T = 0.34$ K data (Fig. 2), only two peaks corresponding to the α-orbit ($f = 265$ T) and β orbit ($f = 470$ T) are observed for a tilt angle of $\theta = 0^\circ$ [shown in the left panel of Fig. 3(a)]. This is due to the elevated temperature as well as the small value of 2 T for the lower bound of the field range since magnetic breakdown only starts to occur at intermediate field values at $T = 1.3$ K and is therefore not so prominent in this QO spectrum. The middle panel then illustrates the angle dependence of the α-orbit and the β-orbit as a quasi-3D map where the FFT amplitude determines the opaqueness. Each QO spectrum of a tilt angle θ was normalized to its maximum value for clarity. The colorbar, displayed to the right of the right panel of Fig. 3, represents the map between opaqueness and normalized FFT amplitude. Also shown in the middle panel are the DFT-calculated angle dependencies of the hole-like (blue) and electron-like (green) parts of the Fermi surface when rotated from the [001] towards the [110] direction. The α-orbit and β-orbit can, therefore, be identified as the extremal area of the individual hole-like pocket and electron-like pocket of the FS in the *ZRA* high-symmetry plane, respectively, when $\mu_0 H \parallel c$ ($\theta = 0^\circ$), as labeled in the inset of Fig. 2. The right panel of Fig. 3(a) shows the QO spectrum for the tilt angle $\theta = 88^\circ$, where two very closely spaced peaks can be seen around ~125 T. Both seem to originate from the electron-like part of the FS of HfSiS when compared to the DFT-calculated angle dependence. We note that the size and shape of the hole pocket (α) are perfectly captured by DFT calculations, while the experimentally determined size of the electron pocket (β) is around 25% smaller for $\mu_0 H \parallel c$ [see Fig. 3(a)]. Like in ZrSiS [18], this disagreement between the experiment and DFT calculations regarding the electron pocket is mainly present for small tilt angles due to the fact that the bulges of the electron pocket are slightly too large in the DFT calculations.

Next, the fundamental orbit γ, previously assigned to an extremal orbit on the hole-like part of the FS located on a plane between the *ZRA* and ΓXM high-symmetry planes [19] is now labeled as δ, and it originates from the hole-like part of the FS in the ΓXM plane near the *X* high-symmetry point. The reason for this reassignment is shown in Fig. 3(b), which displays the angle dependence of the experimentally observed 30 T orbit (labelled as δ) in the field range 4–17 T. The right and the left panels of Fig. 3(b), again, show the QO spectrum for the tilt angles $\theta = 0^\circ$ and $\theta = 88^\circ$, respectively. The middle panel shows the quasi-3D map of the full angle dependence for frequencies below 100 T. The different QO spectra for individual tilt angles are normalized as previously described, but now FFT amplitudes equal to or larger than 0.2 are mapped to complete opaqueness to be able to highlight the experimental angle dependence of the δ-orbit. DFT calculations overestimate the size of this pocket by almost 50% and in contrast to the experimental observations, DFT is not

able to capture the lower frequency branch originating from the δ-orbit between $\theta = 15$–60°.

It is worth noting that there is no experimental evidence for the presence of an ellipsoidal electron-like pocket located at the Γ point (labeled ε in the inset of Fig. 2) in the dHvA QO data [19]. One might suggest that the 30 T frequency originates from this ellipsoidal pocket, but then the area and therefore the observed frequency should increase instead of decrease with increasing tilt angle since this ellipsoidal pocket is expected to be elongated along the [001] direction. Furthermore, there should be no sign of a second branch and therefore it is clear that the observed 30 T frequency and its two branches at larger tilt angles belong to the hole-like part of the Fermi surface in the ΓXM plane near the *X* point. Moreover, the β-orbit is well resolved in both dHvA and SdH QO experiments [19], in stark contrast to the sister compound ZrSiS, where the extremal orbit of the electron "dog-bone" pocket can only be identified unambiguously in the dHvA signal [18].

The FFT spectrum illustrated in Fig. 2 contains besides the observed fundamental orbits numerous other peaks which we divide into two groups: $(*)$ orbits below $f < 1.2\,\mathrm{kT}$ and $(**)$ orbits with frequencies in the range $7.2\,\mathrm{kT} < f < 9.5\,\mathrm{kT}$. Peaks within group $(*)$, labeled by Arabic numbers 1 to 6, are the result of MB between the α and β orbits in the *ZRA* plane. From now on we will refer to this as low-frequency MB and describe the observed peaks of group $(*)$ as different combinations of α and β orbits, namely $n\beta - p\alpha$, for nonzero integers n and p and with the sign indicating electron-like (positive) or hole-like (negative) character. The cyclotron masses were determined by analyzing the QO signals' temperature and field dependence presented at the end of this paper. Group $(**)$, the high-frequency MB labeled with Roman numerals I to VIII, originates from MB in the *ZRA* plane, enclosing the entire nodal-loop at the top of the BZ, which we discuss in detail in the next section. We note that both groups $(*)$ and $(**)$ can only occur between the closely spaced fundamental orbits in the *ZRA* plane for a small region around perfect alignment ($\mu_0 H \parallel c$). Rotating away from the plane (see Fig. S2) causes these orbits to disappear due an increase of the gap Δk that separates the α and β-pockets in k-space with larger tilt angle. This causes the tunneling probability to drop exponentially ($\propto e^{-H_0/H}$, with $H_0 \propto \Delta k^2$), see the SM of Ref. [19] for a detailed discussion.

IV. HIGH-FREQUENCY MAGNETIC BREAKDOWN

We now consider the high-frequency dHvA QOs, group $(**)$, which is the main focus of this work. First reported with limited resolution in our previous SdH study [19], these oscillations are visible for $\mu_0 H > 15$ T and are highlighted in the upper-right inset of Fig. 1(a). Numerous peaks that correspond to breakdown orbits are already visible in the FFT spectrum from 2–32 T in Fig. 2 at 0.34 K. In the following, we assign all high-frequency peaks, labeled with Roman numbers, to MB orbits in the *ZRA* plane by extracting their cyclotron masses from temperature-dependent dHvA QO experiment following the procedure that was successfully employed for ZrSiS [18]. No signatures of MB were found in the ΓXM plane since the k-space gaps are too large for MB to occur.

Figures 4(a) and 4(b) show the corresponding spectra of the FFT obtained from the dHvA studies at 0.34 K and 10 K, respectively, taken in the range 20–32 T (black curves) and 14–19 T (orange curves). The low-temperature FFT spectrum shows in total ten peaks, labeled with Roman numbers from I to X with increasing frequency, summarized in Table II. The two additional peaks in comparison with Fig. 2 are the result of choosing a different field window in which the high-frequency MB is present. The most prominent peak at 0.34 K is peak VI ($f = 8650\,\mathrm{T}$), which prevails also at 10 K. The field-range-dependent evolution of the high-frequency spectrum while varying the upper field value or the lower field value can be found in Figs. S3 and S4 of the SM [23], respectively.

The separation in frequency between the different high-frequency peaks is illustrated by the dashed lines in Fig. 4(a). We first focus on the left part of the high-frequency spectrum, peaks I to VI. All these peaks are separated by a value of $\simeq$265 T, i.e., the frequency of the α-orbit. This separation is indicated with blue dashed lines. From this we can already infer that the high-frequency MB orbits I to V are generated from a base MB orbit that has electron-like character. Only in this scenario, the MB orbits I to V that include more and more α orbits can properly take into account the negative sign of the area of the hole-like α-orbit. Turning our attention now to peaks VI, VIII, and X, we observe that the distance between them corresponds to a value of $\simeq$470 T, i.e., the frequency of the β-orbit. We indicate this with green dashed lines for peaks VIII and X and note that this further confirms the assumption of an electron-like base high-frequency MB orbit, as this correctly matches the addition of the positively signed area of the electron-like β-orbit. As peak VI seems to separate the beginning of both behaviors, i.e., either including an α-orbit and a decrease in frequency, or including a β-orbit and an increase in frequency, we identify it for now as the base high-frequency MB orbit and mark it with a red dashed line. Lastly, we can explain peaks VII and IX by simply noting that they originate from their respective peaks to the right, i.e., peak VIII and X, as the separation between both peak pairs is, again, given by the α-orbit. Now, given the well-resolved high-frequency oscillations in the *ZRA* plane, we show the temperature-dependent QO data and their respective fits using the standard Lifshitz-Kosevich (LK) analysis for the thermal damping factor R_T of QOs (see Ref. [17]) R_T for three selected peaks of the high-frequency MB orbits in Figs. 4(c) to 4(e). For peaks I and X, the insets in Figs. 4(c) and 4(e) describe one of the possible realizations of these high-frequency breakdown orbits, whereas peak VI only has a single realization. The grey shaded empty k-space area enclosed by all individual pockets in the *ZRA* high-symmetry plane is denoted by *A*. In Fig. 4(f) we show the cyclotron masses m_c of all high-frequency MB orbits (summarized in Table II). As for ZrSiS [18], we identify the peak with the lowest cyclotron mass of the dHvA oscillations as the base orbit of the high-frequency spectrum. Here for HfSiS, this is peak VI ($f = 8650\,\mathrm{T}$) with $m_c = (0.73 \pm 0.02) m_e$, which proves our claim of identifying peak VI as base high-frequency orbit. Moreover, we define this base orbit as $A + 4\beta$ [see Fig. 4(d)]. This is justified as only then will this base high-frequency MB orbit have the same cyclotron direction as the fundamental

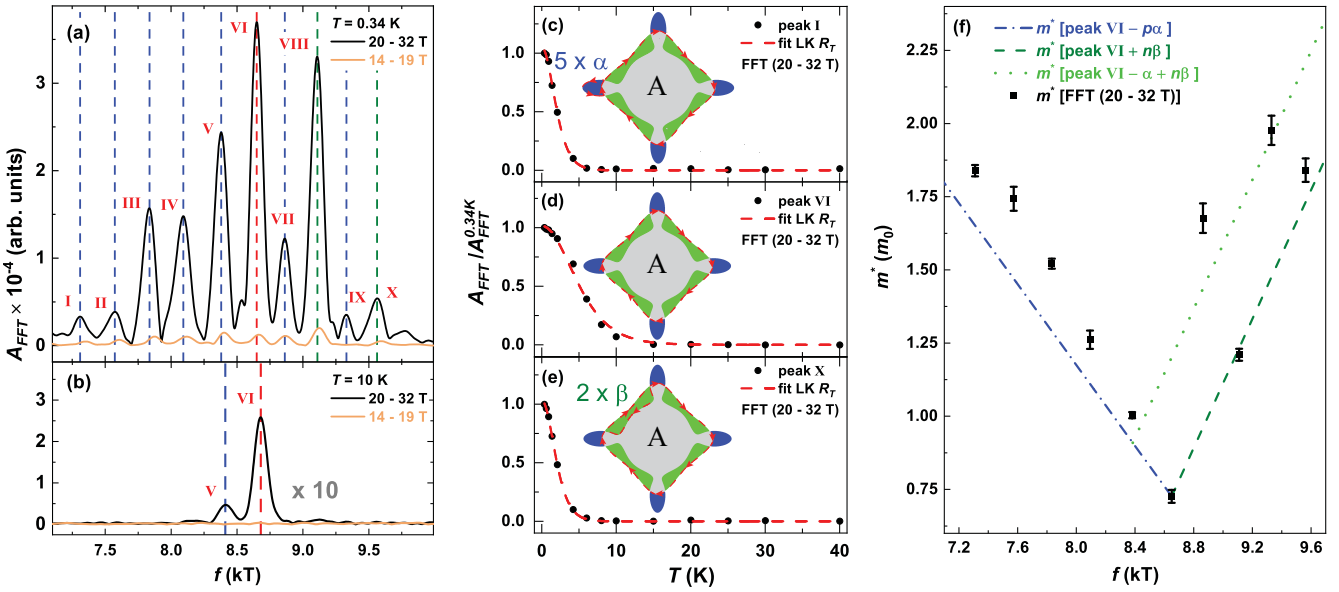

FIG. 4. High-frequency FFT spectrum of the dHvA QOs in the field ranges 20–32 T (black curves) and 14–19 T (orange curves) at (a) $T = 0.34$ K and at (b) $T = 10$ K with the individual peaks (high-frequency MB orbits) labeled by Roman numbers. Data in (b) are multiplied by a factor of 10 for clarity. The dashed lines (a) and (b) indicate the peak positions. The red dashed line indicates the electron-like base high-frequency MB orbit (peak VI). A blue/green dashed line indicates that hole/electron-like character (α-/β-orbit) is added to the nearest peak to the right/next-nearest peak to the left. Shifts in peak positions are due to different field ranges and temperatures (see SM [23]). (c)–(e) Temperature dependence of the FFT amplitudes for peaks I (7310 T), VI (8650 T), and X (9564 T) and the respective fits to the temperature reduction factor R_T of the Lifshitz-Kosevich (LK) expression. Insets in (c) and (e) sketch one realization of each respective high-frequency MB orbit in the *ZRA* high-symmetry plane and also highlight the enclosed empty k-space area A. (f) Cyclotron masses m_c for the MB orbits. The three lines refer to the expected cyclotron masses of the three different series present: $VI - p\alpha$ (dash-dotted blue line), $VI + n\beta$ (dashed dark green line), and $VI - \alpha + n\beta$ (dotted light green line).

β-orbit and therefore, be electron-like. The remaining peaks I to V and VII to X can then be expressed in the general form of $(A + 4\beta) + n\beta - p\alpha$ where the integer pair (n, p) counts the number of additional windings around an β- and/or α-orbit, respectively. The pairs $(0, p)$ with $p = 1$–5 describe peaks V to I, while the pairs $(n, 0)$ peak VIII ($n = 1$) and peak X ($n = 2$). Peak VII is then given by ($n = 1$, $p = 1$) and peak XI is given by ($n = 2$, $p = 1$). Figure 4(f) also confirms our assignment as the cyclotron masses of the individual pockets are added when n and/or p increase and therefore follow the theory of MB (see the SM of Ref. [19] for a derivation and Ref. [24]). We are also able to estimate the size of the empty k-space area A to be 6760 T by subtracting four times the frequency of the β orbit from the frequency of peak VI. This experimental value for A is almost the same as the one found for ZrSiS in Ref. [18] indicating that the Fermi surface at the BZ edge is not significantly different from the one of ZrSiS.

TABLE II. High-frequency MB orbits in the *ZRA* plane, labeling, corresponding cyclotron masses, numbers of tunneling events, avoided tunneling events, and statistical weight factor.

Label	f (T)	Assignment	m_c (m_e)	n_{pj}	n_{qj}	w_j/m_j
I	7310	$(A + 4\beta) - 5\alpha$	1.84 ± 0.02	8	10	1024
II	7575	$(A + 4\beta) - 4\alpha$	1.74 ± 0.04	8	8	256
III	7835	$(A + 4\beta) - 3\alpha$	1.52 ± 0.02	8	6	64
IV	8095	$(A + 4\beta) - 2\alpha$	1.26 ± 0.03	8	4	16
V	8380	$(A + 4\beta) - \alpha$	1.00 ± 0.01	8	2	4
VI	8650	$(A + 4\beta)$	0.73 ± 0.02	8	0	1
VII	8865	$(A + 4\beta) + \beta - \alpha$	1.68 ± 0.05	8	4	16
VIII	9110	$(A + 4\beta) + \beta$	1.21 ± 0.02	8	2	4
IX	9330	$(A + 4\beta) + 2\beta - \alpha$	1.98 ± 0.05	8	6	64
X	9565	$(A + 4\beta) + 2\beta$	1.84 ± 0.04	8	4	16

Our assignment of the high-frequency MB series originating from the base orbit $(A + 4\beta)$ fits the picture perfectly, which is proven by the agreement between the experiment and semiclassical MB theory for cyclotron masses of peaks VII to X. However, we note that there is a slight enhancement of the experimentally found cyclotron mass for peaks I to V. Taking into account that, according to semiclassical MB theory, the Fermi surface of HfSiS in the *ZRA* plane also allows for a second, hole-like base orbit with a cyclotron mass which is approximately three times larger than the cyclotron mass of the $(A + 4\beta)$ base orbit, may account for the observed enhancement. This second, hole-like base MB orbit is constructed from the area A and the four α orbits; we denote it as $(A + 4\alpha)$. A quick check reveals that the frequency of $(A + 4\alpha)$ is 7830 T which, for us, is indistinguishable from peak III $[(A + 4\beta) - 3\alpha]$ at 7835 T. This, then may also explain why peak III is still quite prominent. Moving on, the high-frequency MB series generated by $(A + 4\alpha)$ is given by $(A + 4\alpha) + p\alpha - n\beta$, but because peak III and $(A + 4\alpha)$ coincide in frequency the two different high-frequency MB series perfectly overlap for peaks III to VI, resulting in a deviation from the expected cyclotron masses for the peaks to the left of peak VI.

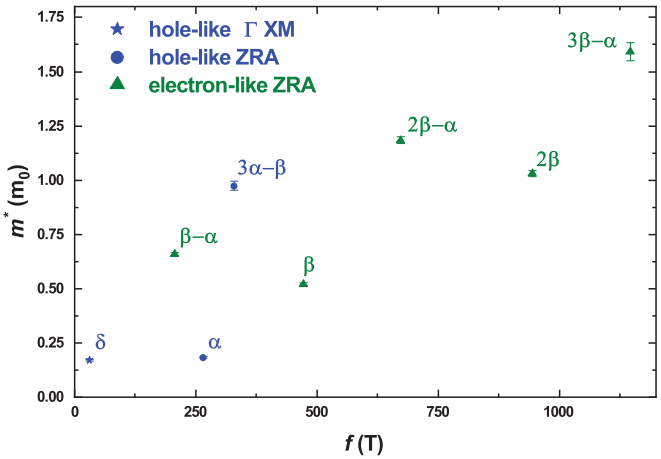

FIG. 5. Cyclotron masses m_c for the individual and low-frequency MB orbits as a function of frequency.

V. LOW-FREQUENCY MAGNETIC BREAKDOWN

Having identified the high-frequency MB orbits, let us now focus on the low-frequency MB referred to as group (∗) in Fig. 2 for frequencies below 1.2 kT. As mentioned before, all these peaks can be identified as linear combinations of f_α and f_β, which we denote as $n\beta - p\alpha$ (summarized in Table S2). The FFTs of these orbits, shown in Figs. S5 and S6 of the SM [23], gradually appear with increasing magnetic field. The oscillation frequency of a specific breakdown orbit is given by the total enclosed area, whereby the areas of the electron and hole pockets contribute with opposite signs (electron-like: positive; hole-like: negative). As in our previous SdH QO data, the simplest semi-classically allowed breakdown orbit is $\beta - \alpha$ ($f = 205$ T) that leads to QOs with a frequency set by the difference between f_β and f_α and is referred to as a "figure-of-eight"-orbit in Ref. [19]. All the other peaks in the FFT spectrum require n and/or p to be greater than unity to form the corresponding low-frequency MB orbit. In total, six pronounced MB orbits with different combinations of $n\beta - p\alpha$ can be identified in Fig. 2: $\beta - \alpha$ ($f = 205$ T), $3\alpha - \beta$ ($f = 325$ T), $4\alpha - \beta$ ($f = 590$ T), $2\beta - \alpha$ ($f = 675$ T), $5\alpha - \beta$ ($f = 850$ T), and $3\beta - \alpha$ ($f = 1145$ T). In Fig. 5 we present the cyclotron masses of the fundamental and low-frequency MB orbits. A more detailed analysis can be found in the SM [23]. Their absolute values are summarized in Tables I and S2. Following the theoretical prediction, the cyclotron masses of the combined electron and hole orbits should add up using Eq. (1) of the SM of Ref. [19]. The only underestimated cyclotron mass is the one of $3\beta - \alpha$ orbit, suggesting that the lower boundary of the field range of the FFT is chosen too low, resulting in an underestimation of its m_c. We note that this specific MB orbit has not been observed in ZrSiS, but is present in HfSiS. The reason for this is that the SOI-enhanced gap in k-space in HfSiS between adjacent individual pockets in the *ZRA* plane leads to a different breakdown probability relative to ZrSiS and therefore does not result in complete destructive interference between different realizations of the $3\beta - \alpha$ orbit (see SM [23] for a detailed description).

To conclude, we presented a high-field study of the dHvA QOs on the NLSM HfSiS. The experimental resolution allowed us to determine the high-frequency QO spectrum originating from MB orbits encircling the nodal-loop in the *ZRA* high-symmetry plane, which is remarkable since HfSiS has a threefold enhanced gap between adjacent electron and hole pockets relative to its sister compound ZrSiS. Furthermore, we found a large number of low-frequency MB orbits while no signatures of MB were found in the ΓMX-plane. Overall, we demonstrated that Dirac NLSMs are an interesting playground to investigate quasi-particle tunneling beyond ZrSiS and that the effect of SOI in this family of materials can be investigated by looking at the presence/absence of certain MB orbits.

ACKNOWLEDGMENTS

This work was supported by HFML-RU/NWO-I, a member of the European Magnetic Field Laboratory (EMFL) and by the UK Engineering and Physical Sciences Research Council (Grant No. EP/R011141/1). This publication is part of the project TOPCORE (OCENW.GROOT.2019.048) of the research program NWO - GROOT, which is financed by the Dutch Research Council (NWO). MB was funded by the German Research Foundation (DFG) through Grant No. 418688556 and the CRC-TR 183 "entangled states of matter." LMS is supported by the Gordon and Betty Moore Foundation's EPIQS initiative through Grant No. GBMF9064.

[1] N. P. Armitage, E. J. Mele, and A. Vishwanath, Weyl and Dirac semimetals in three-dimensional solids, Rev. Mod. Phys. **90**, 015001 (2018).

[2] C. Fang, H. Weng, X. Dai, and Z. Fang, Topological nodal line semimetals, Chin. Phys. B **25**, 117106 (2016).

[3] Y. Huh, E.-G. Moon, and Y.-B. Kim, Long-range Coulomb interaction in nodal-ring semimetals, Phys. Rev. B **93**, 035138 (2016).

[4] J. Liu and L. Balents, Correlation effects and quantum oscillations in topological nodal-loop semimetals, Phys. Rev. B **95**, 075426 (2017).

[5] B. Roy, Interacting nodal-line semimetal: Proximity effect and spontaneous symmetry breaking, Phys. Rev. B **96**, 041113(R) (2017).

[6] L. M. Schoop, M. N. Ali, C. Straßer, A. Topp, A. Varykhalov, D. Marchenko, V. Duppel, S. S. P. Parkin, B. V. Lotsch, and C. R. Ast, Dirac cone protected by non-symmorphic symmetry and three-dimensional Dirac line node in ZrSiS, Nat. Commun. **7**, 11696 (2016).

[7] M. Neupane, I. Belopolski, M. M. Hosen, D. S. Sanchez, R. Sankar, M. Szlawska, S.-Y. Xu, K. Dimitri, N. Dhakal, P. Maldonado, P. M. Oppeneer, D. Kaczorowski, F. Chou, M. Z.

Hasan, and T. Durakiewicz, Observation of topological nodal fermion semimetal phase in ZrSiS, Phys. Rev. B **93**, 201104(R) (2016).

[8] X. Wang, X. Pan, M. Gao, J. Yu, J. Jiang, J. Zhang, H. Zuo, M. Zhang, Z. Wei, W. Niu, Z. Xia, X. Wan, Y. Chen, F. Song, Y. Xu, B. Wang, G. Wang, and R. Zhang, Evidence of both surface and bulk dirac bands and anisotropic nonsaturating magnetoresistance in ZrSiS, Adv. Electron. Mater. **2**, 1600228 (2016).

[9] M. N. Ali, L. Schoop, C. Garg, J. M. Lippmann, E. Lara, B. Lotsch, and S. Parkin, Butterfly magnetoresistance, quasi-2D Dirac Fermi surface and topological phase transition in ZrSiS, Sci. Adv. **2**, e1601742 (2016).

[10] J. Hu, Z. Tang, J. Liu, Y. Zhu, J. Wei, and Z. Mao, Nearly massless Dirac fermions and strong Zeeman splitting in the nodal-line semimetal ZrSiS probed by de Haas-van Alphen quantum oscillations, Phys. Rev. B **96**, 045127 (2017).

[11] R. Singha, A. Pariari, B. Satpati, and P. Mandal, Large nonsaturating magnetoresistance and signature of nondegenerate Dirac nodes in ZrSiS, Proc. Natl. Acad. Sci. **114**, 2468 (2017).

[12] J. Hu, Z. Tang, J. Liu, X. Liu, Y. Zhu, D. Graf, K. Myhro, S. Tran, C.-N. Lau, J. Wei, and Z. Mao, Evidence of Topological Nodal-Line Fermions in ZrSiSe and ZrSiTe, Phys. Rev. Lett. **117**, 016602 (2016).

[13] A. Topp, J. M. Lippmann, A. Varykhalov, V. Duppel, B. V. Lotsch, C. R. Ast, and L. M. Schoop, Non-symmorphic band degeneracy at the Fermi level in ZrSiTe, New J. Phys. **18**, 125014 (2016).

[14] S. Pezzini, M. R. van Delft, L. M. Schoop, B. V. Lotsch, A. Carrington, M. I. Katsnelson, N. E. Hussey, and S. Wiedmann, Unconventional mass enhancement around the Dirac nodal loop in ZrSiS, Nat. Phys. **14**, 178 (2018).

[15] Y. Shao, A. N. Rudenko, J. Hu, Z. Sun, Y. Zhu, S. Moon, A. J. Mills, S. Yuan, A. I. Lichtenstein, D. Smirnov, Z. Q. Mao, M. I. Katsnelson, and D. N. Basov, Electronic correlations in nodal-line semimetals, Nat. Phys. **16**, 636 (2020).

[16] L. Aggarwal, C. K. Singh, M. Aslam, R. Singha, A. Pariari, S. Gayen, M. Kabir, P. Mandal, and G. Sheet, Tip-induced superconductivity coexisting with preserved topological properties in line-nodal semimetal ZrSiS, J. Phys.: Condens. Matter **31**, 485707 (2019).

[17] D. Shoenberg, *Magnetic Oscillations in Metals* (Cambridge University Press, Cambridge, England, 1984).

[18] C. S. A. Müller, T. Khouri, M. R. van Delft, S. Pezzini, Y.-T. Hsu, J. Ayres, M. Breitkreiz, L. M. Schoop, A. Carrington, N. E. Hussey, and S. Wiedmann, Determination of the Fermi surface and field-induced quasi-particle tunneling around the Dirac nodal-loop in ZrSiS, Phys. Rev. Res. **2**, 023217 (2020).

[19] M. R. van Delft, S. Pezzini, T. Khouri, C. S. A. Müller, M. Breitkreiz, L. M. Schoop, A. Carrington, N. E. Hussey, and S. Wiedmann, Electron-Hole Tunneling Revealed by Quantum Oscillations in the Nodal-Line Semimetal HfSiS, Phys. Rev. Lett. **121**, 256602 (2018).

[20] D. Takane, Z. Wang, S. Souma, K. Nakayama, C. X. Trang, T. Sato, T. Takahashi, and Y. Ando, Dirac-node arc in the topological line-node semimetal HfSiS, Phys. Rev. B **94**, 121108(R) (2016).

[21] C. Chen, X. Xu, J. Jiang, S.-C. Wu, Y. P. Qi, L. X. Yang, M. X. Wang, Y. Sun, N. B. M. Schröter, H. F. Yang, L. M. Schoop, Y. Y. Lv, J. Zhou, Y. B. Chen, S. H. Yao, M. H. Lu, Y. F. Chen, C. Felser, B. H. Yan, Z. K. Liu *et al.*, Dirac line nodes and effect of spin-orbit coupling in the nonsymmorphic critical semimetals MSiS (M = Hf, Zr), Phys. Rev. B **95**, 125126 (2017).

[22] N. Kumar, K. Manna, Y. Qi, S.-C. Wu, L. Wang, B. Yan, C. Felser, and C. Shekhar, Unusual magnetotransport from Si-square nets in topological semimetal HfSiS, Phys. Rev. B **95**, 121109(R) (2017).

[23] See Supplemental Material at http://link.aps.org/supplemental/10.1103/PhysRevResearch.4.043008 for which includes a description of sample synthesis and structural characterization, experimental details and analysis, electronic structure calculations, angle dependence of the quantum oscillations, cyclotron mass analysis, a field-range analysis of low- and high-frequency magnetic breakdown quantum oscillations, as well as a theoretical description of the amplitude of the low-frequency breakdown orbit $3\beta - \alpha$.

[24] M. I. Kaganov and A. A. Slutskin, Coherent magnetic breakdown, Phys. Rep. **98**, 189 (1983).